On the effect of dispersed phase viscosity and mean residence time on the Droplet Size Distribution for High-shear Mixers.

DOI:
10.1016/j.ces.2017.07.002

Document Version
Accepted author manuscript

On the effect of dispersed phase viscosity and mean residence time on the Droplet Size Distribution for High-shear Mixers.

Sergio Carrillo De Hert, Thomas L. Rodgers*

School of Chemical Engineering and Analytical Science, The University of Manchester, Manchester M13 9PL, U.K.

Abstract

Properties of emulsified product such as stability, rheology and interfacial area dependent on their micro-structure, specially their mean droplet size and droplet size distribution. Mechanistic models in literature focus on predicting the maximum droplet diameter or Sauter mean diameter but not in their size distribution. The effect of viscosity (9.58-295 mPa s), mean residence time and stirring speed (50-150 s^{-1}) have been investigated using an in-line laboratory scale rotor-stator and dilute (negligible coalescence) coarse emulsions with seven Silicon Oils of different viscosity.

Low viscous oils produced monomodal distributions whereas the ones for intermediate and high viscous oils were bimodal. The mode or modes of the distributions were used for the modelling of the large and small daughter droplet sizes. The droplet size modelling had a mean absolute error (MAE) of 8%. To model the distributions by volume two Generalized Gamma functions were used and fitted using the least absolute error. The distributions were reasonably well-described while predicting the Sauter mean diameter of both mono and bimodal distributions with a MAE of 13.8%.

Keywords: Emulsification, Dispersed Phase Viscosity, Bimodal Size Distribution, Droplet Size Distribution, Rotor-stator mixer, Droplet Break-up Mechanism

*Corresponding author: +44 (0)161 306 8849

Email addresses: sergio.carrillodehert@manchester.ac.uk (Sergio Carrillo De Hert), tom.rodgers@manchester.ac.uk (Thomas L. Rodgers)

Nomenclature

Latin symbols

$\dot{Q}$	volumetric flow rate [$m^3\,s^{-1}$]
$\overline{d}_{30}$	volume arithmetic mean [µm]
$\overline{d}_{32}$	Sauter mean diameter [µm]
$\overline{t}_{res}$	mean residence time [s]
A_i	ith fitting constant [-]
$C_{L,j}$	fitting constant for large daughter droplet correlation for variable j [-]
$C_{s,j}$	fitting constant for small daughter droplet for variable j [-]
CI	confidence interval [-]
D	diameter of the impeller [m]
d_i	diameter of the ith droplet [µm]
d_{max}	maximum droplet diameter [µm]
E	energy density [$J\,kg^{-1}$]
$f_v(d_i)$	frequency by volume of the droplets of the ith diameter [-]
MAE	mean absolute error [%]
Mo	mode [µm]
Mo_L	mode of the large daughter droplets [µm]
Mo_s	mode of the small daughter droplets [µm]
N	stirring speed [s^{-1}]
n	number of passes [-]
n_{ri}	refractive index [-]
P	power draw [W]
$P_n(d_i)$	probability by number of droplets of ith size [%]
$P_v(d_i)$	probability by volume of droplets of ith size [%]
$P_{v,L}(d_i)$	probability of large daughter droplets of ith size [%]
$P_{v,s}(d_i)$	probability of small daughter droplets of ith size [%]
$P_{v,T}(d_i)$	total probability of droplets of ith size [%]
pn	pump number [-]
R^2	coefficient of determination [-]
s	specific gravity [-]
V	swept volume [m^3]

Greek symbols

α	parameter in the Fréchet probability density function [-]
β	parameter in the Fréchet probability density function [-]
η	Kolmogorov length scale [m]
κ	broadness parameter in the Generalized Gamma distribution [-]
λ	scale parameter in the Generalized Gamma distribution [-]
μ_c	viscosity of the continuous phase [Pa s]
μ_d	viscosity of the dispersed phase [Pa s]
$\overline{\varepsilon}$	mean energy dissipation rate per unit mass of fluid [$W\,kg^{-1}$]
ϕ_L	volume fraction of the large daughter droplets [-]
ϕ_s	volume fraction of the small daughter droplets [-]
ρ_c	density of the continuous phase [$kg\,m^{-3}$]
ρ_d	density of the dispersed phase [$kg\,m^{-3}$]
σ	interfacial tension [N m]
σ_d	standard deviation of the normal distribution [µm]
$\sigma_{\log(d)}$	standard deviation of the log-normal distribution [µm]
τ	skewness parameter in the Generalized Gamma distribution [-]
ε	energy dissipation rate per unit mass of fluid [$W\,kg^{-1}$]
ε_m	maximum energy dissipation rate per unit mass of fluid [$W\,kg^{-1}$]

Dimensionless numbers

Po	Power number $PN^{-3}D^{-5}\rho^{-1}$

Abbreviations

DSD	droplet size distribution
GGd	Generalized Gamma distribution
SLES	Sodium Laureth Sulfate

Introduction

High-shear mixers are able to create small droplets with large interfacial areas due to their localized energy dissipation rates, high rotor speeds and the narrow spacing between the rotor and the stator. These mixers are widely used to produce cosmetics, foods, paints, pharmaceuticals and chemical (Zhang et al., 2012; Atiemo-Obeng and Calabrese, 2003), but despite their wide applicability there is almost no fundamental understanding on these devices (Atiemo-Obeng and Calabrese, 2003). The two main types of high-shear mixers used are the radial discharge batch and the in-line rotor-stators. In-line rotor-stators allow for continuous processing and offer versatility to change from one product formulation to another using the same equipment by valve switching.

The droplet size distribution (DSD) of an emulsion affects its stability (Ma et al., 2005), rheology (Derkach, 2009) and absorption in drug delivery systems (Ma et al., 2010). For example, narrow DSDs are less susceptible to coalescence and Ostwald ripening; therefore personal care products with broad DSD are stabilized by large amounts of surfactants which may cause irritation, skin drying and allergic reactions (Nazir et al., 2013). The rheology of emulsions depends on the droplet-droplet interactions and droplet deformability among other parameters, which are a function of viscosity (both phases), volume fraction, mean droplet size and their DSD (Derkach, 2009); this is important in products such as paint (Watson and Mackley, 2002).

In this study we deal with dilute systems; for these systems drop coalescence is considered negligible and drop breakage can be isolated for its study. Mechanistic models assume that equilibrium for these systems is reached

when all of the drops are smaller than a maximum stable drop size d_{max} (Leng and Calabrese, 2003). A linear relationship betwen d_{max} and the Sauter mean diameter $\overline{d}_{32}$ was proposed by Shinnar (1961) and has been used by many authors

$$\overline{d}_{32} = A_1 d_{max} \tag{1}$$

The Sauter mean diameter is one of the most important measures of central tendency used in emulsification technology because it is inversely proportional to the interfacial area of a given distribution. The previous relationship makes $\overline{d}_{32}$ and d_{max} in all the models presented in Sections 2.1 and 2.2 interchangeable. The equations below show how $\overline{d}_{32}$ is calculated if the number frequency $f_n(d_i)$ or the volume frequency $f_v(d_i)$ are given.

$$\overline{d}_{32} = \frac{\sum_{i=1} f_n(d_i) d_i^3}{\sum_{i=1} f_n(d_i) d_i^2} = \frac{\sum_{i=1} f_v(d_i)}{\sum_{i=1} \frac{f_v(d_i)}{d_i}} \tag{2}$$

Where d_i is the ith droplet diameter.

As many emulsions may have the same d_{max} and/or $\overline{d}_{32}$ but different DSD, it is highly desirable to obtain a model which describes the whole distribution, specially when the DSD are bimodal.

Theoretical background

Mechanistic models

It is widely accepted that in turbulent flow droplets can break by two types of stresses depending on the droplets size in relation with the size of

the smallest possible eddies. According to Kolmogorov (1949) the length scale of the smallest eddies η for isotropic turbulence is given by

$$\eta = \left(\frac{\mu_c}{\rho_c}\right)^{\frac{3}{4}} \varepsilon^{-\frac{1}{4}} \tag{3}$$

Where μ_c and ρ_c are the viscosity and density of the continuous phase and ε is the local energy dissipation rate which value depends on the location of the tank, thereby it is more convenient to use the average energy dissipation rate $\overline{\varepsilon}$ or the maximum energy dissipation rate ε_m, both being proportional for geometrically similar systems (Leng and Calabrese, 2003)

$$\varepsilon_m \propto \overline{\varepsilon} \propto \frac{P}{\rho_c V} \propto \frac{\mathrm{Po}\rho_c N^3 D^5}{\rho_c D^3} \propto \mathrm{Po} N^3 D^2 \tag{4}$$

Where P is the power consumption, V is the volume of the vessel and Po is the dimensionless power number ($\mathrm{Po} = P/\rho_c N^3 D^5$). For a geometrically similar mixers and constant Po: $\varepsilon \sim N^3 D^2$ where N is the impeller speed and D its diameter. The aforementioned stresses are either due to hydrodynamic fluctuations when the droplets are larger than η or by viscous stresses when these are smaller.

The maximum drop diameter d_{max} in the inertia regime according to the Kolmogorov-Hinze theory is (Kolmogorov, 1949; Hinze, 1955):

$$d_{max} \propto \left(\frac{\sigma}{\rho_c}\right)^{\frac{3}{5}} \varepsilon^{-\frac{2}{5}} \tag{5}$$

Where σ is the interfacial tension. The previous equation was obtained by balancing the disruptive forces ($\propto (\varepsilon d)^{2/3}$) and the capillary pressure inside

the droplet ($4\sigma d^{-1}$). Equation 5 does not take into account the viscosity of the dispersed phase μ_d and is considered valid only for the inviscid droplets or when μ_d is small. Davies (1985) included a viscous resistance inside the deforming droplet and Calabrese et al. (1986) expanded the model by doing a balance of the disruptive turbulent energy obtaining

$$d_{max} = A_1 \left(\frac{\sigma}{\rho_c}\right)^{\frac{3}{5}} \varepsilon^{-\frac{2}{5}} \left[1 + A_2 \left(\frac{\rho_c}{\rho_d}\right)^{\frac{1}{2}} \frac{\mu_d \varepsilon^{\frac{1}{3}} d_{max}^{\frac{1}{3}}}{\sigma}\right]^{\frac{3}{5}} \tag{6}$$

Where ρ_d is the density of the dispersed phase and A_i $(i = 1, 2, ...)$ are fitting constants.

In the turbulent viscous regime $d_{max} < \eta$, in this range μ_c is no longer negligible (as in Eq. 6) as viscous stresses may add to inertial stresses. Two sets of mechanistic models can be derived in this regime depending on the type of stresses considered: inertial stresses for $d_{max} < \eta$ and viscous stress for $d_{max} \ll \eta$. For inertial stresses in the turbulent viscous regime (Padron, 2005)

$$d_{max} = A_3 \left(\frac{\sigma \mu_c}{\rho_c^2 \varepsilon}\right)^{\frac{1}{3}} \left[1 + A_4 \frac{\mu_d \rho_c}{\sigma} \left(\frac{\varepsilon}{\rho_d \mu_c}\right)^{\frac{1}{2}} d_{max}\right]^{\frac{1}{3}} \tag{7}$$

If viscous stresses inside the turbulent eddies act as the disruptive forces, according to Shinnar (1961) these are $\sim (\varepsilon \rho_c \mu_c)^{1/2}$. The balance of the disruptive force, capillary forces and viscous forces inside the droplet yield (Padron, 2005)

$$d_{max} = A_5 \frac{\sigma}{(\varepsilon \mu_c \rho_c)^{\frac{1}{2}}} \left[1 + A_6 \frac{\mu_d}{\sigma} \frac{(\mu_c \rho_c)^{\frac{1}{4}}}{\rho_d^{\frac{1}{2}}} \varepsilon^{\frac{1}{4}}\right] \tag{8}$$

Table 1: Summary of limits of the Mechanistic Models and power law indexes on studied variables.

		Limit	**Model**		**Index**	
		$\mu_d \rightarrow$	$d_{max} \propto$		μ_d	N
Supra-Kolmogorov	Inertia sub-range (Eq. 6)	0	$\left(\frac{\sigma}{\rho_c}\right)^{3/5} \varepsilon^{-2/5}$	(9)	0	$-6/5$
		∞	$\left[\frac{\mu_d}{(\rho_c \rho_d)^{1/2}}\right]^{3/4} \varepsilon^{-1/4}$	(10)	3/4	$-3/4$
Sub-Kolmogorov	Inertia stress model (Eq. 7)	0	$\left(\frac{\sigma \mu_c}{\rho_c^2}\right)^{1/3} \varepsilon^{-1/3}$	(11)	0	-1
		∞	$\left[\left(\frac{\mu_d}{\rho_c}\right)^2 \frac{\mu_c}{\rho_d}\right]^{1/4} \varepsilon^{-1/4}$	(12)	1/2	$-3/4$
	Viscous stress model (Eq. 8)	0	$\frac{\sigma}{(\mu_c \rho_c)^{1/2}} \varepsilon^{-1/2}$	(13)	0	$-3/2$
		∞	$\frac{\mu_d}{\left(\rho_d^2 \mu_c \rho_c\right)^{1/4}} \varepsilon^{-1/4}$	(14)	1	$-3/4$

The limits for $\mu_d \rightarrow 0$ (inviscid limit) and $\mu_d \rightarrow \infty$ of the three mechanistic models presented in Equations 6, 7 and 8 are shown in Table 1. The present study is focused on μ_d, N and $\bar{t}_{res}$ on the Droplets Size Distribution. The same table shows that according to the mechanistic models, μ_d's power law dependency for highly-viscous oils ranges from 0.5 to 1 and N's index ranges from -0.75 to -1.5.

Atiemo-Obeng and Calabrese (2003) estimated that stirred vessels are usually not operated at a sufficient high power draw to produce droplets of the length of η. Rueger and Calabrese (2013) experimented with a high-shear mixer and found that their data were well correlated by the sub-Kolmogorov inertia stress mechanistic models whereas Hall et al. (2011) obtained droplets

of the order of magnitude of η and none of the mechanistic models described their results, this was attributed to the homogeneous isotropic turbulence assumption which is unlikely for rotor-stators.

Multi-pass emulsification

The mechanistic models above assume that the equilibrium DSD has been reached, nevertheless in in-line rotor-stators the residence time is usually insufficient to reach equilibrium and further drop breakage occurs for multiple passes. Jasińska et al. (2014); Håkansson et al. (2016) and Carrillo De Hert and Rodgers (2017) performed experiments for $n = 10$, 8 and 20 respectively and were unable to reach steady-state. Two different approaches for multipass experiments for in-line rotor-stators have been reported in literature. The first one is the energy density E proposed by Karbstein and Schubert (1995)

$$\overline{d}_{32} \propto E^{A_7} \propto \left(\overline{\varepsilon}\overline{t}_{res}\right)^{A_7} \tag{15}$$

Making $\overline{t}_{res} = Vn/\dot{Q}$ where V is the swept volume (Hall et al., 2013), n is the number of passes through the rotor-stator and $\dot{Q}$ is the volumetric flow rate throw the rotor-stator. Substituting Equation 4 in the previous equation we obtain

$$\overline{d}_{32} \propto \left(P\frac{n}{\dot{Q}}\right)^{A_7} \tag{16}$$

For a in-line rotor-stator P is a function of $\dot{Q}$, N, the equipment and the properties of the materials being processed, a method to obtain P can be found in (Kowalski, 2009).

Hall et al. (2011, 2013) could not fit their results using Equation 16. Hall et al. (2013) proposed a second correlation based on tip speed (ND) and $\bar{t}_{res}$

$$\overline{d}_{32} \propto (ND)^{A_8} \left(\frac{n}{\dot{Q}}\right)^{A_9} \tag{17}$$

They found that A_9 decreased as μ_d increased, they found $A_9 = -0.148$ for the 9.4×10^{-3} Pa s silicon oil and $A_9 = -0.043$ for the 3.39×10^{-1} Pa s one. Hall et al. (2011) found that $\overline{d}_{32} \propto \dot{Q}^{-0.19}$. In our previous work (Carrillo De Hert and Rodgers, 2017) we found that the mode Mo was more useful than $\overline{d}_{32}$ to track emulsification kinetics and that the DSDs were homoscedastic and hence $d_{max} \propto Mo$. We could not fit the Mo of our DSD using Equation 16 either, nevertheless Equation 17 provided a good fit, making $A_8 = -1.2$ and $A_9 = -0.2$ we obtained $R^2 = 0.985$ and a mean error of 4.7% for 78 DSDs (n and $\dot{Q}$ varied systematically) using a 9.580×10^{-3} Pa s silicon oil.

Droplet Size Distribution

For A_1 in Equation 1 Sprow (1967) found $A_1 = 0.38$. Calabrese et al. (1986) determined that A_1 decreases as μ_d increases, they found $A_1 = 0.59$ for $\mu_d = 1 \times 10^{-1}$ Pa s and $A_1 = 0.52$ for $\mu_d = 10$ Pa s. Rueger and Calabrese (2013) obtained $A_1 = 0.49$. Li et al. (2014) found that $A_1 = 0.16$, they attributed the discrepancy to the bimodality of the DSD they obtained. Liu et al. (2013) also studied bimodal DSD and found that A_1 decreased from 0.225 to 0.130 as the viscosity of the dispersed phase increased from 9.6×10^{-3} Pa s to 4.25×10^{-1} Pa s, but was independent on N and volume fraction.

Chen and Middleman (1967) fitted a normal distribution to their DSD by volume.

$$P_v\left(\frac{d_i}{\overline{d}_{32}}\right) = \frac{1}{\sqrt{2\pi}\sigma_d}\exp\left[\frac{\left(\frac{d_i}{\overline{d}_{32}} - \frac{\overline{d}_{30}}{\overline{d}_{32}}\right)^2}{2\sigma_d^2}\right] \tag{18}$$

Where $P_v\left(d_i/\overline{d}_{32}\right)$ is the normalized volume probability density, σ_d its standard deviation and $\overline{d}_{30}$ is the volume arithmetic mean.

Calabrese et al. (1986) and Vankova et al. (2007) used similar expressions to fit the volume DSD. Nevertheless Calabrese et al. (1986) found that for high viscosities the DSDs broaden and could be better described by a number log-normal distribution.

$$P_n(d_i) = \frac{1}{\sqrt{2\pi}\sigma_{\log(d)}}\exp\left\{-\frac{\left[\log(d_i) - \overline{\log\left(d_i\right)}\right]^2}{2\sigma_{\log(d)}^2}\right\} \tag{19}$$

Where $P_n\left(d_i\right))$ is the number probability density, $\sigma_{\log(d)}$ its standard deviation and $\overline{\log\left(d_i\right)}$ the geometric mean.

Li et al. (2014) emulsified a $1.14 \times 10^{-1}\,\mathrm{Pa\,s}$ crude oil in water using a rotor-stator at different N and volume fraction and obtained bimodal DSDs. They transformed the DSD by volume into a number distribution. This operation gives higher weight to the smallest droplet, and this conversion resulted in a monomodal DSD by number. They further used three different probability density functions to fit the DSD by number; namely a normal, a log-normal and a Fréchet distribution. The Fréchet distribution provided the best fit.

$$P_n(d_i) = \frac{\alpha}{\beta}\left(\frac{\beta}{d_i}\right)^{\alpha+1}\exp\left[-\left(\frac{\beta}{d_i}\right)^{\alpha}\right] \tag{20}$$

Where α and β are obtained using the Equations below

$$\beta^{\alpha} = \frac{n}{\sum_{i=1}^{n} \frac{1}{d_i^{\alpha}}} \tag{21}$$

$$\frac{n}{\alpha} + n \ln \beta - \sum_{i=1}^{n} \ln d_i - \sum_{i=1}^{n} \left(\frac{\beta}{d_i}\right)^{\alpha} \ln \left(\frac{\beta}{d_i}\right) = 0 \tag{22}$$

The same fit was used by Liu et al. (2013) for a variety of bimodal emulsions obtained using a rotor-stator and silicon oils in the 9.6×10^{-3} Pa s-4.26×10^{-1} Pa s viscosity range.

Materials and equipment and methods

Materials

For each experiment 10 L of coarse emulsion was prepared using different Silicon Oils. The Silicon Oil concentration of the emulsions was 1% by volume and 1% by weight of surfactant.

Texapon N701 (Cognis Ltd., Hertfordshire, U.K.) was used used as surfactant. Texapon contains $\approx 70\%$ concentration by weight of sodium laureth sulfate (SLES) and $\approx 30\%$ water and impurities. SLES is an anionic surfactant consisting of mixture of alkyl ether sulphates (C_{12-14}) with EO sodium salt. Its molar mass and specific gravity s are $420\,\mathrm{g\,mol^{-1}}$ and 1.03 respectively (EL-Hamouz et al., 2009).

Six 200 Silicone Fluid (dimethyl siloxane, Dow Corning, Michigan, U.S.A.) of different viscosity were used as dispersed phase. Additionally, a blend of the 1000 cSt and 10000 cSt Silicon Oils was made to obtain an oil of intermediate viscosity, this oil was labelled as 2760 cSt. The specific gravity s,

dynamic viscosity μ_d, interfacial tension σ of the Silicon Oil-1% SLES/water solution, and refractive index n_{ri} of the seven oils are listed in Table 2.

Table 2: Relevant properties of the Silicon Oils used at 25 °C.

Silicon Oil [cSt]	s [-]	μ_d [Pa s]	σ [N m]	n_{ri} [-]
10	0.934	9.580×10^{-3}	8.809×10^{-3}	1.399
50	0.960	4.913×10^{-2}	9.096×10^{-3}	1.402
350	0.965	3.279×10^{-1}	9.129×10^{-3}	1.403
1000	0.970	9.474×10^{-1}	9.172×10^{-3}	1.404
2760	0.970	2.745×10^{0}	-	1.404
10000	0.970	1.051×10^{1}	-	1.404
30000	0.970	2.951×10^{1}	-	1.404

The specific gravities listed are the ones found in the material's Safety Data Sheet (SDS); the viscosities were determined experimentally using a DV2T Viscometer (Brookfield Vicometers, Essex, U.K.) in a water bath; the interfacial tension was measured using a platinum-iridium KRUSS standard ring (KRUSS GmbH, Hamburg, Germany) and a K11 Mk4 Tensiometer (KRUSS GmbH, Hamburg, Germany); and the refractive indexes using a RFM390 Refractometer (Bellingham & Stanley Ltd, Kent, UK). The σ for Silicon Oils with $\mu_d > 9.474 \times 10^{-1}$ Pa s could not be measured using the available Du-Noüy ring method; nevertheless, as the change of σ as μ increases is small, it is assumed constant for the most viscous oils. As shown in Table 2, Silicon Oils allow to study the effect of the dispersed phase viscosity on the DSD as these are available in a wide range of viscosities while having similar s, σ and n_{ri}.

Equipment and methods

The equipment used for this study has been thoroughly described in (Carrillo De Hert and Rodgers, 2017) for the continuous arrangement. A L5M-A Laboratory Mixer (Silverson Machines Ltd, Chesham, U.K.) was used for this study. The rotor used had four blades, an external diameter of 30 mm, blade thickness of 5 mm and a height of 10 mm. The screen used had 240 holes in 6 rows of 40 holes each in pitch arrangement. Its external diameter, height and thickness were 32 mm, 20 mm and 1 mm respectively. The Power number Po for this rotor-stator has been previously determined to be 0.215 in Ref. (Carrillo De Hert and Rodgers, 2017).

A peristaltic pump (501 single channel pumphead, Watson Marlow, Cornwall, U.K.) with arbitrary pump number ranging from 1 to 999 was used to push the coarse emulsion through the L5M-A Laboratory Mixer (Silverson Machines Ltd, Chesham, U.K.) working at a established impeller speed N. The output was collected in a second 12 L vessel. For experiments involving multiple passes, the feed and collection tank were swapped and the process was repeated for n number of passes.

The coarse emulsions were prepared by dissolving 142.94 g of Texapon N701 in 9.77 L of water in an unbaffled 12 L cylindrical vessel using a 6-blade Rushton impeller with 6 cm of diameter. Once the surfactant had been completely dissolved, 0.100 L of Silicon Oil were poured slowly while the vessel was being stirred at a rotational speed $N = 6.4\,\mathrm{s}^{-1}$. The emulsions were stirred for 24 h to guarantee that the coarse emulsion fed to the rotor-stator had the same drop size and DSD (see supplementary material 1). The stirring speed in the vessel was lowered to $N = 3.3\,\mathrm{s}^{-1}$ while the coarse

emulsion was pumped through the rotor-stator to ensure that further droplet burst was only due to the action of the rotor-stator while keeping the coarse emulsion homogeneous within the vessel.

Samples for each pass through the rotor-stator were immediately analysed in a Mastersizer 3000 (Malvern Instruments, Malvern, U.K.). The n_{ri} used for each Silicon Oil are shown in Table 2, while the one used for water was 1.333. The absorption index used for all Silicon Oils was 10^{-3} following Malvern's suggestion. Each sample was analysed 5 times and at least three samples were analysed; the arithmetical average of the 15 distributions was obtained and are the DSD reported in this study.

The experiments in this study focus on the effect of μ, $\bar{t}_{res}$ and N on the DSD. Experiments for $n = 1, 2, ..., 8$, keeping $N = 150\,\mathrm{s}^{-1}$ and $\dot{Q} = 2.217 \times 10^{-5}\,\mathrm{m}^3\,\mathrm{s}^{-1}$ constant using the Silicon Oils previously listed in Table 2 were performed. For the 1000 cSt Silicon Oil ($\mu = 9.474 \times 10^{-1}\,\mathrm{Pa\,s}$) additional experiments varying $\dot{Q}$ were performed for $n = 1, 2, ..., 8$ keeping $N = 150\,\mathrm{s}^{-1}$. Lastly, the effect of N for three Silicon Oils was studied for $n = 1$ and $\dot{Q} = 2.217 \times 10^{-5}\,\mathrm{m}^3\,\mathrm{s}^{-1}$. For this N range all the experiments are in the turbulent regime (constant Po) (Carrillo De Hert and Rodgers, 2017).

The experimental matrix can be seen in Table 3. The first experiments performed were the ones varying μ_d for constant N and $\dot{Q}$. The results obtained for these experiments were analysed before doing the rest of the experiments. The effect of N, n and $\dot{Q}$ for the 10 cSt Silicon Oil have been previously reported by Carrillo De Hert and Rodgers (2017) using the same equipment. As will be seen in Section 4, the experiments using the 350 cSt Silicon Oil yielded DSD where the two distributions of the daughter droplets

Table 3: Experimental matrix. X denoted the experiments performed.

μ_d [Pa s]	$n = 1, 2, ..., 8$ $N = 150\,\mathrm{s}^{-1}$ $\dot{Q}/10^{-5}$ [$\mathrm{m}^3\,\mathrm{s}^{-1}$]				$n = 1$ $\dot{Q}/10^{-5} = 2.217\,\mathrm{m}^3\,\mathrm{s}^{-1}$ N [s^{-1}]				
	0.908	1.506	2.217	2.897	50	75	100	125	150
9.580×10^{-3}	-	-	X	-	-	-	-	-	-
4.913×10^{-2}	-	-	X	-	X	X	X	X	X
3.279×10^{-1}	-	-	X	-	-	-	-	-	-
9.474×10^{-1}	X	X	X	X	X	X	X	X	X
2.745	-	-	X	-	X	X	X	X	X
1.051×10^{1}	-	-	X	-	-	-	-	-	-
2.951×10^{1}	-	-	X	-	-	-	-	-	-

were not distinguishable and thus no more experiments using this oil were done. For two thickest oils did not follow the model proposed for the 10 cSt-2 760 cSt Silicon Oils, and thus no further experiments were performed because thicker oils were unavailable.

Results and discussion

Phenomenology

The DSDs by volume obtained for the experiments at constant $\dot{Q}$ and N for $n = 1, 2, ..., 8$ for all the silicon oils are shown in Figure 1. Figures 1a and 1b show one distinctive peak whereas the DSDs for the 350 cSt Silicon Oil (Fig. 1c) have a broader DSD than the obtained for the previously mentioned oils. Furthermore, the DSD is not symmetrical and as will be discussed later, this was attributed to the presence of two types of daughter droplets namely the large and small daughter droplets. Thicker oils (Figs. 1d-1g) showed a clear bi-modality. Figures 1d-1f show that the distribution of the small

daughter drops is broader than the one of the large ones, they also show that as viscosity increases the peaks get further apart: (1) the size of the large droplets increase and (2) the small daughter droplets become smaller. Therefore the asymmetrical shape of the DSDs obtained for the 350 cSt oil was attributed to the distributions of the large and small droplets being close together. From this it can be inferred that a change of the droplet break-up mechanism occurs for a viscosity between 50 cSt and 350 cSt.

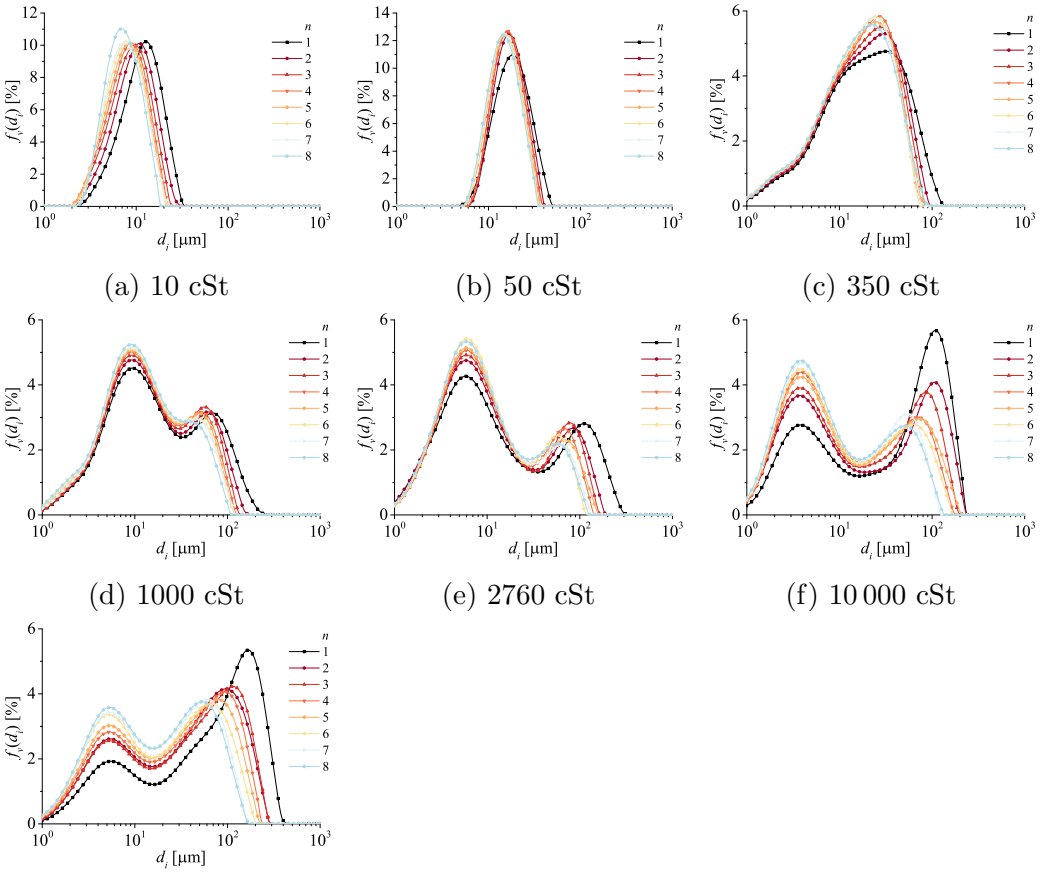

(a) 10 cSt (b) 50 cSt (c) 350 cSt

(d) 1000 cSt (e) 2760 cSt (f) 10 000 cSt

(g) 30 000 cSt

Figure 1: DSDs obtained for all Silicon Oils for $n = 1, 2, .., 8$, $\dot{Q} = 2.217 \times 10^{-5}\,\mathrm{m^3\,s^{-1}}$ and $N = 150\,\mathrm{s^{-1}}$.

For the 30 000 cSt (Fig. 1g) it can be seen than small daughter droplets are larger than the ones obtained using the 10 000 cSt oil, reversing the trend found for the 350 cSt-10 000 cSt viscosity range. Furthermore, the shape of the DSDs in Figure 1g suggest that a third distribution may be present (best observable for $n = 1$).

Figs. 1a and 1b shows that as n ($\propto \bar{t}_{res}$) increases the droplets become smaller, this is also true for the large daughter droplets in Figures 1c-1g, suggesting that the large daughter droplets are generated by the same break-up mechanism that gave birth to the ones for the 10cSt and 50 cSt oils. From Figures 1d-1g it can also be observed that n has no influence on the size of the small daughter droplets, but do increase their quantity.

In their study on the effect of viscosity on the DSD for stirred vessels, Calabrese et al. (1986) reported a transition from a monomodal to a bimodal DSD for silicon oils with a $\mu \geq 1\,\mathrm{Pa\,s}$ which was attributed to a transition from a bursting to a transition breakage mechanism. For the bimodal DSDs they noted that as viscosity increases the DSD broadens as the small droplets become smaller and the large larger. This is in agreement with the results obtained in this study, however the appearance of the two types of droplets may appear at viscosities lower than $\mu_d \geq 3.279 \times 10^{-1}\,\mathrm{Pa\,s}$. On the other hand, Hall et al. (2011) reported that for an in-line rotor-stator both types of daughter droplets increased in size with viscosity which is in disagreement with the findings in this study.

Most of the DSD obtained allow for the Mode Mo of one or two distributions to be obtained; the exception being the DSD obtained for the 350 cSt where two distributions are merged and produce a distribution with an

single mode.

The Mo of the large Mo_L and small Mo_s daughter droplets of the DSDs presented in Figure 1 are shown in Figure 2 as a function of n and in Figure 3 as a function of μ_d. The results presented in Figure 2a for the most viscous Silicon Oils are scattered due to the difficulty in analysing the samples, nevertheless Figure 2a shows that Mo_L decreases in size as n increases and Figure 2b that its effect on Mo_s is negligible.

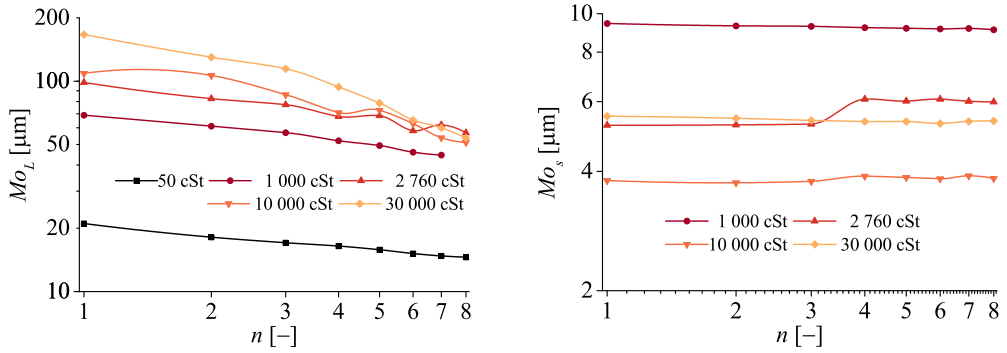

(a) (b)

Figure 2: Effect of n for constant for $\dot{Q} = 2.217 \times 10^{-5}\,\mathrm{m^3\,s^{-1}}$ and $N = 150\,\mathrm{s^{-1}}$ on (a) Mo_L and (b) Mo_s.

Figure 3 shows Mo_L for $n = 1, 2, .., 8$ and the averaged Mo_s for all n (Mo_s independent on n). Mo_L first increases with viscosity and then plateaus, on the other hand Mo_s decreases with viscosity and suddenly increases for the most viscous Silicon Oil, suggesting a change in the break-up mechanism. The index found for the large and small daughter droplets were 0.37 and -0.37 respectively. Suggesting that the droplets increase and decrease in size at the same rate respectively.

The power law index found in our study is in disagreement with any of

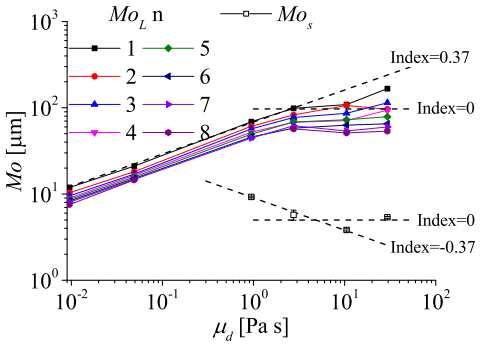

Figure 3: Mo_L (closed symbols) for $n = 1, 2, ...8$ and averaged Mo_s (open symbols) as a function of μ_d for $\dot{Q} = 2.217 \times 10^{-5}\,\mathrm{m^3\,s^{-1}}$ and $N = 150\,\mathrm{s^{-1}}$

the three mechanistic models (Eqs. 6, 7 and 8 and Tab. 1) reviewed in Section 2. The estimated $\eta = 6.3\,\mu\mathrm{m}$ which in the order of magnitude of the d_{max} obtained for the two thinnest oils (See Figs. 1a and 1b), implying that either the Supra-Kolmogorov inertia sub-range or the Sub-Kolmogorov inertia stress model should apply. As shown in Table 1, the expected viscosity dependence index should be either 1/2 or 3/4, which are significantly higher than the 0.37 found in this study. Thicker oils have a $d_{max} > \eta$ and no change in slope was obtained.

The studies found in literature on the effect of μ_d on the DSD use d_{max} or $\overline{d}_{32}$ as parameter. It is important to mention that if the shape (broadness and skewness) of the distribution of the large daughter droplets is independent on property materials and processing parameters, the trends found in this study for Mo_L should be similar to the ones for d_{max}, not to $\overline{d}_{32}$. The $\overline{d}_{32}$ includes both types of daughter droplets, meaning that it is affected by their size, volume fraction and distribution shape unless the DSDs are monomodal and homoscedastic.

Arai K. et al. (1977) used Polystyrene in the 7.8×10^{-4} Pa s-1.5 Pa s viscosity range as dispersed phase to study the d_{max} dependency on μ_d. He found that for 7.8×10^{-4} Pa s $> \mu_d > 7.8 \times 10^{-2}$ Pa s the droplet sizes did not vary; droplet size increased with μ_d until a 0.75 power-law index was reached for 2×10^{-1} Pa s $> \mu_d > 1.5$ Pa s, finally a decrease in the index for polystyrene with $\mu_d > 1.5$ Pa s was found. Ludwig et al. (1997) used a screw loop reactor to emulsify paraffin oils in the 3.2×10^{-2} Pa s-1.9×10^{-1} Pa s in water and SDS (Sodium dodecyl sulfate) as emulsifier. They found the same trend as Arai K. et al. (1977) but the d_{max} dependency on μ_d started to level off at μ_d values as low as $\mu_d \geq 1.9 \times 10^{-1}$ Pa s. Liu et al. (2013) developed a model based on the one of Calabrese et al. (1986) that accounts for dispersed phase volume fraction and dispersed phase viscosity, their model suggests that $d_{max} \propto \mu_d^{0.6}$. Our results follow the trend found in previous studies in that the droplet sizes increase with viscosity and then levels off, but does not agree on the power-law index value.

Arai K. et al. (1977) and Padron (2005) suggested that when μ_d is relatively small deformed drops can restore their spherical shape faster than the more viscous drops. Because viscous drops have a longer deformation time-scale, it is difficult to restore their equilibrium shape and thus several eddies may elongate the drops consecutively forming threads before bursting. The higher the viscosity the longer these threads are and therefore more and smaller satellite drops will be generated. This droplet break-up mechanisms resembles the ones for laminar shear flows known as capillary-wave instability or Rayleigh instability. Eastwood et al. (2004) used high-speed video images to study the breakup of materials in the 5×10^{-4} Pa s-5.09×10^{-2} Pa s viscos-

ity range using a prototypical set-up with a turbulent water jet. They found that droplets stretch dramatically before rupture and that the stretching increases with viscosity.

Figure 4 shows the $\overline{d}_{32}$ as a function of μ_d for $n = 1, 2, ..., 8$. As expected, $\overline{d}_{32}$ increases with viscosity for the oils producing monomodal DSDs ($\mu_d = 9.580 \times 10^{-3}\,\mathrm{Pa\,s}$ and $\mu_d = 4.913 \times 10^{-2}\,\mathrm{Pa\,s}$). For $4.913 \times 10^{-2}\,\mathrm{Pa\,s} > \mu_d > 1.051 \times 10^{1}\,\mathrm{Pa\,s}$ decreases in a power-law fashion. The gradual decline in $\overline{d}_{32}$ in this viscosity range is due to the decrease in size of the small daughter droplets which have a stronger effect on $\overline{d}_{32}$ than the large daughter droplets. For $\mu_d = 2.951\,\mathrm{Pa\,s}$ the trend shot up, the cause being the increase in size of the small daughter droplets (see Fig. 3).

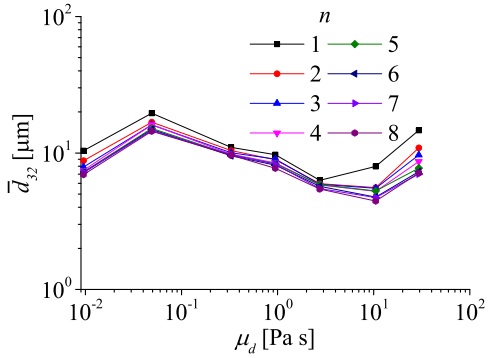

Figure 4: $\overline{d}_{32}$ as a function μ_d for $n = 1, 2, ..., 8$, $\dot{Q} = 2.217 \times 10^{-5}\,\mathrm{m^3\,s^{-1}}$ and $N = 150\,\mathrm{s^{-1}}$.

Hall et al. (2011) and Padron (2005) studied the effect of viscosity on the DSD using a batch and in-line rotor-stator respectively. Both authors found a $\overline{d}_{32}$ increase with viscosity followed by a plateau and the appearance of a second distribution for the most viscous oils. Wang and Calabrese (1986) dispersed Silicon Oils in the $1 \times 10^{-3}\,\mathrm{Pa\,s}$-$1\,\mathrm{Pa\,s}$ viscosity range in several

ethanol in water solutions. They also found that a 0.75 power law index described the $\overline{d}_{32}$ dependency on μ_d for intermediate viscosity silicon oils. They could fit their data to an equation similar to Equation 6 but had to exclude the results for the 1 Pa s. EL-Hamouz et al. (2009) found a 0.46 power law index dependency of $\overline{d}_{32}$ on μ_d for silicon oils in the 4.9×10^{-4} Pa s-3.4×10^{-1} Pa s viscosity range using a pitched blade turbine and a sawtooth impeller. The studies mentioned on the effect of $\overline{d}_{32}$ are in disagreement with our results as was shown in Figure 4.

Figures 5a and 5b depict the effect of N. The former shows the effect of N on the DSD for the 1 000 cSt Silicon Oil for a single pass and constant $\dot{Q}$. This figure shows that as N increases the size of both types of daughter droplets decrease in size and that the amount of small daughter droplets increases. This is further shown in the later Figure for different μ_d.

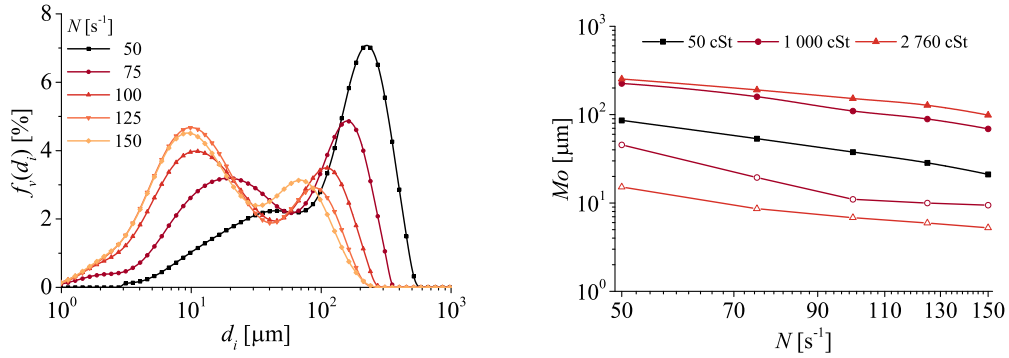

(a) (b)

Figure 5: (a) DSD for the 1 000 cSt Silicon Oil for different impeller speeds N and constant $\dot{Q} = 2.217 \times 10^{-5}\,\mathrm{m^3\,s^{-1}}$ and $n = 1$. (b) Mo_L (closed symbols) and Mo_s (open symbols) as a function of N for constants $\dot{Q} = 2.217 \times 10^{-5}\,\mathrm{m^3\,s^{-1}}$ and $n = 1$.

Droplet size modelling

Provided that most of the DSDs obtained allow to obtain one or two Mo, power law dependencies on μ, N and $\bar{t}_{res}$ ($\bar{t}_{res} \propto n/\dot{Q}$) were proposed

$$Mo_L = C_{L,0}\mu^{C_{L,\mu}} N^{C_{L,N}} \left(\frac{n}{\dot{Q}}\right)^{C_{L,\bar{t}}} \tag{23}$$

$$Mo_s = C_{s,0}\mu^{C_{s,\mu}} N^{C_{s,N}} \left(\frac{n}{\dot{Q}}\right)^{C_{s,\bar{t}}} \tag{24}$$

For Mo_L it was found that the power model proposed described the data obtained for the 10 cSt - 2 760 cSt Silicon Oils while failing to describe the results for the two most viscous oils as $C_{L,\mu} = 0$ (see Fig. 3). Multivariable linear and transformed power regressions were performed to obtain the value of the constants and their 95% confidence intervals CI: $C_{L,0} = 1.14 \times 10^5 \pm 43.3\%$, $C_{L,\mu} = 0.365 \pm 6.24\%$, $C_{L,N} = -1.06 \pm 12.5\%$ and $C_{L,\bar{t}} = -0.192 \pm 24.6\%$. The coefficient of determination R^2 obtained was 0.958 and the mean absolute error MAE was 8.74%. Carrillo De Hert and Rodgers (2017) found that $C_{L,\bar{t}} = -0.2$ for the a larger set of experiments using the same 10 cSt Silicon Oil and the same equipment used for this study. To homologate both studies, the fit for $C_{L,\bar{t}}$ was forced to -0.2, the corrected value for the other constants are shown in Table 4. The result obtained was a fit with an $R^2 = 0.959$ and $MAE = 8.71\%$.

Table 4: Fitting constants for Eqs. 23 and 24 and their 95% CI.

x	$C_{x,0}$	$C_{x,\mu}$	$C_{x,N}$	$C_{x,\bar{t}}$	MAE
L	$1.18 \times 10^5 \pm 41.2\%$	$0.365 \pm 6.18\%$	$-1.05 \pm 10.3\%$	$-0.2*$	8.71%
s	1.69×10^3	$-0.365*$	$-1.05*$	$0*$	7.47%

$*$ fixed values.

Analogously for Mo_s the regression yielded $C_{s,0} = 1.16 \times 10^3 \pm 50.6\%$, $C_{s,\mu} = 0.385 \pm 10.3\%$, $C_{s,N} = -1.02 \pm 15.8\%$ and $C_{s,\bar{t}} = -0.0211 \pm 242\%$. The fit yielded $R^2 = 0.851$ and an $MAE = 8.24\%$. As $C_{s,\mu} \sim -C_{L,\mu}$, $C_{s,N} \sim C_{L,N}$ these term were assumed equal and $C_{s,\bar{t}}$ was assumed to be zero as its value is small and its CI is large. The new values for the constants in Equation 24 can also be consulted in Table 4; the R^2 and MAE were 0.884 and 7.47% respectively.

The Goodness of the fit for both types of daughter droplets is showed in Figure 6.

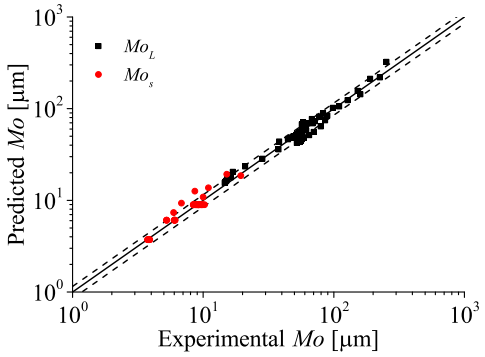

Figure 6: Goodness of the fit using Eqs. 23 and 24 and the constant values in Tab. 4. The dashed lines represent 15% error.

Our model suggest that bimodality surges when Mo_L and Mo_s acquire the same value; when the lines in Figure 3 intercept; the constants obtained in Table 4 suggest that bimodality is independent on N but dependent on $\bar{t}_{res}$:

$$\mu = 3 \times 10^{-3} \left(\frac{n}{\dot{Q}} \right)^{0.274} \tag{25}$$

For example, for $n = 1$ and $\dot{Q} = 2.217 \times 10^{-5}\,\mathrm{m^3\,s^{-1}}$, Equation 25 suggests

that small daughter droplets will be present for $\mu > 5.65 \times 10^{-2}\,\mathrm{Pa\,s}$. As $t_{res} \propto {}^{n}/_{\dot{Q}}$, equation 25 also suggests that the appearance of small daughter droplets for a given viscosity occur for small t_{res} as the Mo of the large daughter droplets approaches the size of the small daughter droplets.

Droplet Size Distribution modelling

As the results obtained from the Mastersizer are reported as frequency distributions by volume $f_v(d_i)$, these were converted into probability density functions $P_v(d_i)$. The conversion was done using the trapezium integration rule.

$$P_v(d_i) = \frac{f_v(d_i)}{\sum_{d_i=0.01\,\mu\mathrm{m}}^{3\times10^3\,\mu\mathrm{m}} \frac{f_v(d_{i+1}) - f_v(d_i)}{2\,(d_{i+1} + d_i)}} \cdot 100 \tag{26}$$

The former equation allows for the area under the distribution, or the total probability to be 100%. The probability density function used for this study is the Generalized Gamma distribution (GGd). This distribution has three parameter: one scale parameter λ and two shape parameters κ and τ; the former is related to the broadness of the distribution and the later to its skewness. Its equation is

$$P_v(d_i) = \frac{\kappa}{\lambda\Gamma(\tau)} \left(\frac{d_i}{\lambda}\right)^{\tau\kappa-1} \exp\left\{-\left(\frac{d_i}{\lambda}\right)^{\kappa}\right\} \tag{27}$$

Two GGd were used when the condition established in Equation 25 was true. To account for the fraction of large and small daughter droplets the parameters ϕ_L and ϕ_s were introduced ($\phi_s = 1 - \phi_L$). The equation for

bimodal distributions thus become

$$P_{v,T}(d_i) = (1 - \phi_s)P_{v,L}(d_i) + \phi_s P_{v,s}(d_i) \tag{28}$$

Where $P_{v,T}(d_i)$ is the probability distribution of the emulsion, $P_{v,L}(d_i)$ and $P_{v,s}(d_i)$ are the probability distributions of the large and small daughter droplets respectively. Each of the two distributions have their own scale and shape parameters.

The modelling consisted of two steps, (1) determining the value of the parameter for $P_{v,L}(d_i)$ and $P_{v,s}(d_i)$ and (2) modelling of ϕ_s.

The effects of μ, N and $n/\dot{Q}$ on the droplet sizes were previously determined to follow Equations 23 and 24. The same power law dependencies as well as $C_{x,\mu}$, $C_{x,N}$ and $C_{x,\bar{t}}$ reported in Table 4 were used for λ_L and λ_s, nevertheless the pre-exponential factors should acquire new values ($C_{L,1}$ and $C_{s,1}$) as the scale of the GGd are affected by its shape factors α and τ

$$\lambda_L = C_{L,1}\mu^{C_{L,\mu}} N^{C_{L,N}} \left(\frac{n}{\dot{Q}}\right)^{C_{L,\bar{t}}} \tag{29}$$

$$\lambda_s = C_{s,1}\mu^{C_{L,\mu}} N^{-C_{L,N}} \tag{30}$$

The DSD for both daughter droplet distributions were assumed to be symmetrical, this is attained by making τ_L and τ_s large; as $\tau \to \infty$ a GGd becomes a normal distribution. Therefore we considered $\tau_L = \tau_s = 10$.

To determine the best values for α_L and α_s we assumed that the broadness of the distributions are constant for all the experiments (shape independent of N, μ and $\bar{t}_{res}$).

Figures 2a and 5a show that the volume fraction of small daughter droplets ϕ_s is affected by μ, n and N. Another power-law dependency was proposed

$$\phi_s = C_{\phi,1}\mu^{C_{\phi,\mu}} N^{\phi,N} \left(\frac{n}{\dot{Q}}\right)^{C_{\phi,\bar{t}}} \tag{31}$$

The fit was carried out by minimizing the absolute error between the re-scaled experimental DSD and Equation 28 for all our experiments (87 DSDs) for the 10 cst-2 760 cSt viscosity range. It was found that the constants in Table 5 produced reasonable results while decreasing the number of variables.

Table 5: Values for the constants $C_{x,y}$ obtained by fitting the DSD using MAE as criteria.

Scale parameters $C_{x,y}$			
	x		
y	L	s	ϕ
1	6.19×10^3	2.63×10^1	1.33×10^{-4}
μ	0.365	-0.365	-0.365
N	-1.05	-1.05	1.05
$\bar{t}$	-0.2	0	0.2
Shape parameters			
α	0.735	0.488	
τ	10	10	

Figure 7 shows how the model fits our results for different viscosities for constant $n = 5$, $\dot{Q} = 2.217 \times 10^{-5}\,\mathrm{m^3\,s^{-1}}$ and $N = 150\,\mathrm{s^{-1}}$. It is worth mentioning that despite discarding the results for the 350 cSt Silicon Oil in the previous sections, the model proposed is capable of estimating the asymmetrical shape of the DSD by volume (see Fig. 7c).

Regarding the region where Mo_L and Mo_s are viscosity independent (plateau in Fig. 3), $C_{L,\mu}$ and $C_{L,\mu}$ become zero in Equations 23 and 24

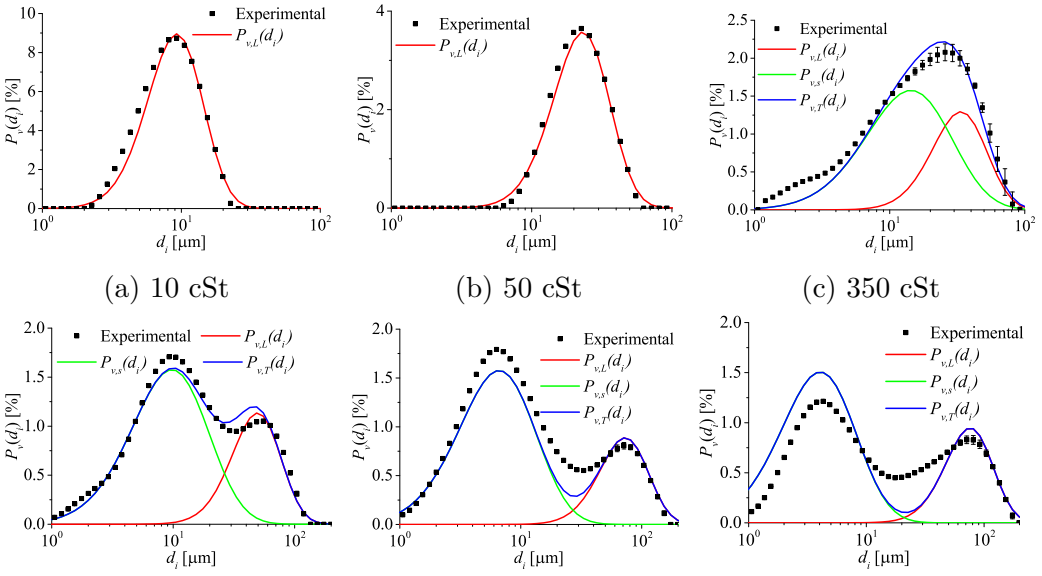

(a) 10 cSt (b) 50 cSt (c) 350 cSt

(d) 1 000 cSt (e) 2 760 cSt (f) 10 000 cSt

Figure 7: Experimental and modelled DSD for 5 Silicon Oils for $n = 5$, $\dot{Q} = 2.217 \times 10^{-5}\,\mathrm{m^3\,s^{-1}}$ and $N = 150\,\mathrm{s^{-1}}$. The error bars represent two standard deviations.

respectively. Assuming that the rest of the power indexes keep the same value $C_{L,0} = 8.41 \times 10^8$ and $C_{s,0} = 9.60 \times 10^2$ with a $MAE = 10.4\%$ for the large daughter droplets and $MAE = 16.9\%$ for the small ones.

The fit shown in Figure 7f for the 10 000 cSt Silicon Oil shows that even though the modes of the DSD and of the fit coincide, the volume fractions do not and that there are droplets present in the valley in-between both types of daughter droplets; this worsens for the 30 000 cSt (not shown).

The Goodness of our model can be further assessed in Figure 8 where the experimental and modelled Sauter mean diameter $\overline{d}_{32}$ are compared.

In Figure 9 a 3-D representations of our model is shown. To enhance visibility, the $P_v(d_i)$ results were transformed into $f_v(d_i)$ doing the inverse operation done previously by Equation 26.

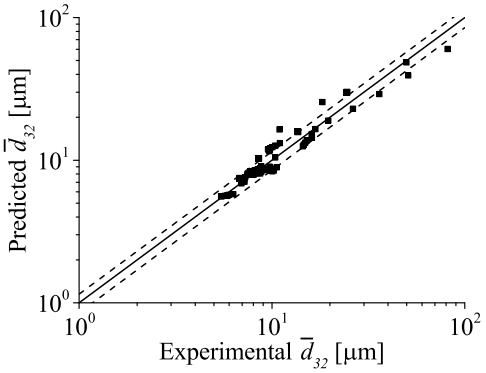

Figure 8: Goodness of the fit considering the Sauter mean diameter $\overline{d}_{32}$ as parameter. The obtained MAE was 9.4%. The dashed lines represent ±15%

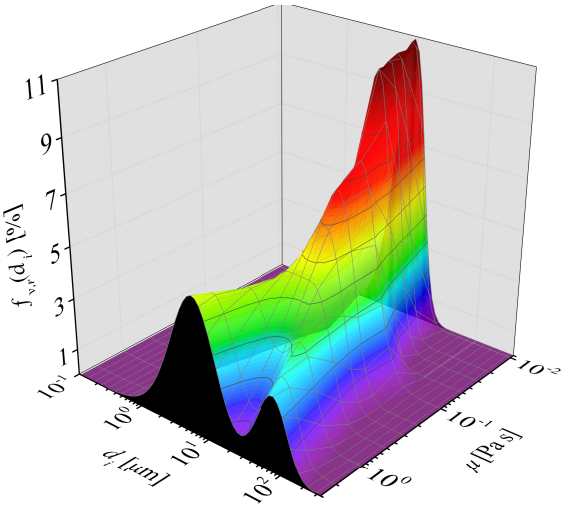

Figure 9: Modelled DSD as a function of μ for $(n/\dot{Q}) = 2 \times 10^5\,\mathrm{s\,m^{-3}}$ and $N = 150\,\mathrm{s^{-1}}$.

Figure 9 shows that as viscosity increases, the DSD evolved from a narrow monomodal distribution into a broader DSD (such as the 350 cSt DSD in Figs. 1c and 7c) and finally into a bimodal DSD. As stated previously, large

and small daughter droplets are present when the condition established by Equation 25 is fulfilled, this is the cause for the sudden drop in $f_v(d_i)$ and increase in broadness. The large and small daughter distributions separate as viscosity increases; the large droplets become larger and the small become smaller at the same rate ($C_{L,\mu}$=-$C_{s,\mu}$). Even though $C_{\phi,\mu}$ is negative, it can be observed that the amount of small daughter droplets increases with viscosity, this is because of the transformation of probability density into a relative frequency.

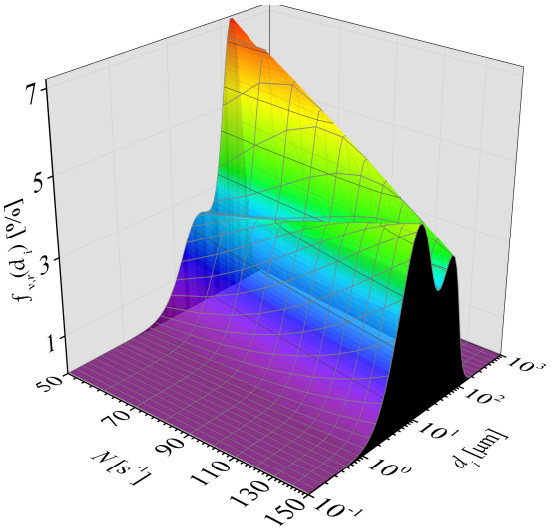

Figure 10: Modelled DSD as a function of N for $\mu = 1\,\mathrm{Pa\,s}$ and $(n/\dot{Q}) = 2 \times 10^5\,\mathrm{s\,m^{-3}}$.

Figure 10 depicts the effect of N on a bimodal DSD. It shows that as N increase the size of both large and small droplets decrease (at the same rate $C_{L,N} = Cs, N$), furthermore has a strong impact on ϕ_s; as N increases so does the amount of small droplets.

The effect of $\bar{t}_{res}$ or $(n/\dot{Q})$ on the DSD is more subtle than the one of

the two aforementioned variables as previously shown in Figure 1; the size of the small daughter droplets is $\bar{t}_{res}$ independent and the large droplets sizes have a -0.2 power dependency. The volume fraction of the small droplets dependency has a 0.2 index.

Conclusions

The effects of dispersed phase viscosity, stirring speed and mean residence time on the droplet size distribution have been investigated with special emphasis on the first by using 7 silicon oils of different viscosity in the 9.58×10^{-3} Pa s-2.95×10^{1} Pa s range. As viscosity increased a transition from monomodal to bimodal distributions was observed, this was attributed to a change in the droplet break-up mechanism. The mode or modes of the DSD were used to characterize the sizes of the large and small daughter droplets under the assumption that the broadness and skewness of the DSD were independent of viscosity.

It was found that the sizes of the large daughter droplets first increased with viscosity with a power law index of 0.37 before levelling off at approximately 2.75 Pa s suggesting a third break-up mechanism. The 0.37 dependency is in disagreement with the one proposed by the mechanistic models. The modes belonging to the small daughter droplets decreased in size at the same rate as the large ones increased.

Furthermore the large daughter droplets decreased in size as the mean residence time increased while the small daughter droplets were unaffected. The power law dependency found was very close to the one found in our previous study Carrillo De Hert and Rodgers (2017) where a more extensive

study on mean residence time was done. The effect of stirring speed affected the sizes of both types of daughter droplets equally with a power law index of $-1.05 \pm 10.3\%$ which is in agreement with the mechanistic models.

Two Generalized Gamma probability density functions were used to fit the DSD by volume. The scale parameter was parametrized using the same power functions used to describe the modes; with a 0.365 viscosity index for viscosities up to 2.745 Pa s and zero for the two most viscous oils. The shape of both types of daughter droplets were assumed symmetrical (in log scale) and thus a large value for τ was fixed. The broadness of the distributions was considered an independent variable but constant throughout the viscosity, mean residence time and stirring speed range. The other independent variable for fitting the DSD was the volume fraction of the small daughter droplets, which was assumed to follow another power function for all variables. The independent variables were adjusted using the minimum absolute error criteria.

For low and intermediate viscosities the fit was successful in that the shape of the DSD is described and in that the MAE of the experimental and predicted $\overline{d}_{32}$ was $MAE = 9.4\%$. As the shape of the large daughter droplets was homoscedastic throughout the viscosity range, the modes are proportional to d_{max}.

However for the most viscous oils, the region in-between the two distributions could not be described with two GGf and the volume fractions of each type of daughter droplets could not be predicted. Further studies could focus on how to predict the DSD for the high viscosity end where an apparent maximum droplet size is reached.

Funding

The authors would like to express their gratitude to the Mexican National Council for Science and Technology (CONACYT) for supporting this project as part of the first author's PhD studies through the CONACYT-The University of Manchester fellowship program.

Acknowledgements

The authors would also like to thank the workshop staff of The University of Manchester's School of Chemical Engineering and Analytical Science for their help with the modifications and maintenance of the equipment.

Bibliography

Arai K., K. M., Y., M., Saito, S., 1977. Effect of dispersed-phase viscosity on the maximum stable drop size for breakup in turbulent flow. Journal of Chemical Engineering of Japan 10 (4), 325–330.
URL http://dx.doi.org/10.1252/jcej.10.325

Atiemo-Obeng, V. A., Calabrese, R. V., 11 2003. Handbook of Industrial Mixing: Science and Practice. John Wiley & Sons, Inc., Ch. 8 Rotor-Stator Mixing Devices, pp. 479–506.

Calabrese, R. V., K., C. T. P., Dang, P. T., apr 1986. Drop breakup in turbulent stirred-tank contactors. part i: Effect of dispersed-phase viscosity. AIChE Journal 32 (4), 657–666.
URL http://dx.doi.org/10.1002/aic.690320416

534 Carrillo De Hert, S., Rodgers, T., 2017. Continuous, recycle and batch
535 emulsification kinetics using a high-shear mixer. Chemical Engineering
536 Science 167, 265 – 277.
537 URL http://www.sciencedirect.com/science/article/pii/S0009250917302671

538 Chen, H. T., Middleman, S., sep 1967. Drop size distribution in agitated
539 liquid-liquid systems. AIChE Journal 13 (5), 989–995.
540 URL http://dx.doi.org/10.1002/aic.690130529

541 Davies, J., 1985. Drop sizes of emulsions related to turbulent energy dissipa-
542 tion rates. Chemical Engineering Science 40 (5), 839–842.
543 URL http://dx.doi.org/10.1016/0009-2509(85)85036-3

544 Derkach, S. R., oct 2009. Rheology of emulsions. Advances in Colloid and
545 Interface Science 151 (1-2), 1–23.
546 URL http://dx.doi.org/10.1016/j.cis.2009.07.001

547 Eastwood, C. D., Armi, L., Lasheras, J. C., mar 2004. The breakup of immis-
548 cible fluids in turbulent flows. Journal of Fluid Mechanics 502, 309–333.
549 URL http://dx.doi.org/10.1017/S0022112003007730

550 EL-Hamouz, A., Cooke, M., Kowalski, A., Sharratt, P., feb 2009. Dispersion
551 of silicone oil in water surfactant solution: Effect of impeller speed, oil vis-
552 cosity and addition point on drop size distribution. Chemical Engineering
553 and Processing: Process Intensification 48 (2), 633–642.
554 URL http://dx.doi.org/10.1016/j.cep.2008.07.008

555 Håkansson, A., Chaudhry, Z., Innings, F., apr 2016. Model emulsions to
556 study the mechanism of industrial mayonnaise emulsification. Food and

Bioproducts Processing 98, 189–195.
URL http://dx.doi.org/10.1016/j.fbp.2016.01.011

Hall, S., Cooke, M., El-Hamouz, A., Kowalski, A., may 2011. Droplet break-up by in-line silverson rotor-stator mixer. Chemical Engineering Science 66 (10), 2068–2079.
URL http://dx.doi.org/10.1016/j.ces.2011.01.054

Hall, S., Pacek, A. W., Kowalski, A. J., Cooke, M., Rothman, D., nov 2013. The effect of scale and interfacial tension on liquid–liquid dispersion in in-line silverson rotor–stator mixers. Chemical Engineering Research and Design 91 (11), 2156–2168.
URL http://dx.doi.org/10.1016/j.cherd.2013.04.021

Hinze, J. O., sep 1955. Fundamentals of the hydrodynamic mechanism of splitting in dispersion processes. AIChE Journal 1 (3), 289–295.
URL http://dx.doi.org/10.1002/aic.690010303

Jasińska, M., Bałdyga, J., Hall, S., Pacek, A. W., oct 2014. Dispersion of oil droplets in rotor–stator mixers: Experimental investigations and modeling. Chemical Engineering and Processing: Process Intensification 84, 45–53.
URL http://dx.doi.org/10.1016/j.cep.2014.02.008

Karbstein, H., Schubert, H., jun 1995. Developments in the continuous mechanical production of oil-in-water macro-emulsions. Chemical Engineering and Processing: Process Intensification 34 (3), 205–211.
URL http://dx.doi.org/10.1016/0255-2701(94)04005-2

Kolmogorov, A., 1949. O droblenii kapel v turbulentnom potoke. Doklady Akademii Nauk SSSR 66 (5), 825–828.

Kowalski, A. J., jan 2009. An expression for the power consumption of in-line rotor-stator devices. Chemical Engineering and Processing: Process Intensification 48 (1), 581–585.
URL http://dx.doi.org/10.1016/j.cep.2008.04.002

Leng, D. E., Calabrese, R. V., 11 2003. Handbook of Industrial Mixing: Science and Practice. John Wiley & Sons, Inc., Ch. 12 Immiscible Liquid-Liquid Systems, pp. 639–754.

Li, M., Liu, C., Liang, C., Liu, C., Li, J., mar 2014. Study of bimodal drop size distributions of emulsion. Journal of Dispersion Science and Technology 35 (3), 397–402.
URL http://dx.doi.org/10.1080/01932691.2013.791989

Liu, C., Li, M., Liang, C., Wang, W., oct 2013. Measurement and analysis of bimodal drop size distribution in a rotor–stator homogenizer. Chemical Engineering Science 102, 622–631.
URL http://dx.doi.org/10.1016/j.ces.2013.08.030

Ludwig, A., Flechtner, U., Prss, J., Warnecke, H.-J., apr 1997. Formation of emulsions in a screw loop reactor. Chemical Engineering & Technology 20 (3), 149–161.
URL http://dx.doi.org/10.1002/ceat.270200302

Ma, G., Gong, F., Hu, G., Hao, D., Liu, R., Wang, R., dec 2005. Multi-scale structures in emulsion and microsphere complex systems. China Particuol-

ogy 3 (6), 296–303.
URL http://dx.doi.org/10.1016/S1672-2515(07)60206-1

Ma, G.-H., Yang, J., Lv, P.-P., Wang, L.-Y., Wei, W., Tian, R., Wu, J., Su, Z.-G., feb 2010. Preparation of uniform microspheres and microcapsules by modified emulsification process. Macromolecular Symposia 288 (1), 41–48.
URL http://dx.doi.org/10.1002/masy.201050206

Nazir, H., Zhang, W., Liu, Y., Chen, X., Wang, L., Naseer, M. M., Ma, G., nov 2013. Silicone oil emulsions: strategies to improve their stability and applications in hair care products. International Journal of Cosmetic Science 36 (2), 124–133.
URL http://dx.doi.org/10.1111/ics.12104

Padron, G. A., 2005. Effect of surfactants on drop size distributions in a batch, rotor-stator mixer. Ph.D. thesis, The University of Maryland.

Rueger, P. E., Calabrese, R. V., nov 2013. Dispersion of water into oil in a rotor–stator mixer. part 1: Drop breakup in dilute systems. Chemical Engineering Research and Design 91 (11), 2122–2133.
URL http://dx.doi.org/10.1016/j.cherd.2013.05.018

Shinnar, R., mar 1961. On the behaviour of liquid dispersions in mixing vessels. Journal of Fluid Mechanics 10 (02), 259.
URL http://dx.doi.org/10.1017/S0022112061000214

Sprow, F., mar 1967. Distribution of drop sizes produced in turbulent liquid—liquid dispersion. Chemical Engineering Science 22 (3), 435–442.
URL http://dx.doi.org/10.1016/0009-2509(67)80130-1

Vankova, N., Tcholakova, S., Denkov, N. D., Ivanov, I. B., Vulchev, V. D., Danner, T., aug 2007. Emulsification in turbulent flow. Journal of Colloid and Interface Science 312 (2), 363–380.
URL http://dx.doi.org/10.1016/j.jcis.2007.03.059

Wang, C. Y., Calabrese, R. V., apr 1986. Drop breakup in turbulent stirred-tank contactors. part ii: Relative influence of viscosity and interfacial tension. AIChE Journal 32 (4), 667–676.
URL http://dx.doi.org/10.1002/aic.690320417

Watson, D. J., Mackley, M. R., jan 2002. The rheology of aqueous emulsions prepared by direct emulsification and phase inversion from a high viscosity alkyd resin. Colloids and Surfaces A: Physicochemical and Engineering Aspects 196 (2-3), 121–134.
URL http://dx.doi.org/10.1016/S0927-7757(01)00813-5

Zhang, J., Xu, S., Li, W., jul 2012. High shear mixers: A review of typical applications and studies on power draw, flow pattern, energy dissipation and transfer properties. Chemical Engineering and Processing: Process Intensification 57-58, 25–41.
URL http://dx.doi.org/10.1016/j.cep.2012.04.004